Rapid Communications

Crystal structures and phase transitions of the van der Waals ferromagnet VI_3

P. Doležal,[1] M. Kratochvílová,[1] V. Holý,[1] P. Čermák,[1] V. Sechovský,[1] M. Dušek,[2] M. Míšek,[2] T. Chakraborty,[3] Y. Noda,[4] Suhan Son,[3,5] and Je-Geun Park[3,5]

[1]*Department of Condensed Matter Physics, Faculty of Mathematics and Physics, Charles University, Ke Karlovu 5, 121 16 Prague 2, Czech Republic*

[2]*Institute of Physics, Academy of Sciences of Czech Republic, v.v.i, Na Slovance 2, 182 21 Prague 8, Czech Republic*

[3]*Center for Correlated Electron Systems, Institute for Basic Science, Seoul 08826, Korea*

[4]*Institute of Multidisciplinary Research for Advanced Materials, Tohoku University, Sendai 980-8577, Japan*

[5]*Department of Physics and Astronomy, Seoul National University, Seoul 08826, Korea*

(Received 10 September 2019; published 19 December 2019)

The results of a single-crystal x-ray-diffraction study of the evolution of the crystal structures of VI_3 with temperature with an emphasis on phase transitions are presented. Some related specific-heat and magnetization data are included. The existence of the room-temperature trigonal crystal structure $R\bar{3}$ (148) has been confirmed. Upon cooling, VI_3 undergoes a structural phase transition to a monoclinic phase at $T_s \sim 79$ K. T_s is reduced in magnetic fields applied along the trigonal c axis. When VI_3 becomes ferromagnetic at $T_{FM1} \sim 50$ K, magnetostriction-induced changes of the monoclinic-structure parameters are observed. Upon further cooling, the monoclinic structure transforms into a triclinic variant at 32 K which is most likely occurring in conjunction with the previously reported transformation of the ferromagnetic structure. The observed phenomena are preliminarily attributed to strong magnetoelastic interactions.

DOI: 10.1103/PhysRevMaterials.3.121401

Recently, van der Waals ferromagnets have been the subject of intensive research due to their potential use in atomically thin devices with spintronic and optoelectronic functionalities [1–4]. Ferromagnetism persisting down to the monolayer limit is an essential ingredient for future spintronic applications. This was probably the main reason why CrI_3 with the highest Curie temperature ($T_C = 61$ K) among the transition-metal trihalides (TX_3) has attracted so much research interest lately [4–13]. On the other hand, VI_3, which has been known since the 1960's [14–17], has only received significant attention for the past year [18–21]. VI_3 is also ferromagnetic (FM) with $T_C \sim 50$ K, slightly lower than CrI_3.

The TX_3 trihalides are frequently dimorphic. Similar to $CrCl_3$ and $CrBr_3$, the low-temperature (LT) phase of CrI_3 is trigonal BiI_3 type with space group $R\bar{3}$ (148) while the high-temperature (HT) structure is monoclinic $AlCl_3$ type [$C2/m$ (12)]. A first-order structure transition between the two crystallographic phases in $CrCl_3$, $CrBr_3$, and CrI_3 occurs at ~240, 420, and 210 K, respectively [5,22].

Much less is known about the crystal structures of the analogous VX_3 compounds. The only unambiguous information available is that, at room temperature (RT), VCl_3 and VBr_3 also possess the rhombohedral structure $R\bar{3}$ (148) [23–25]. Papers on VI_3, rapidly appearing within a short period, have provided contradictory statements. Son *et al.* [18] report the RT trigonal structure $P\bar{3}1c$ (163), a structural phase transition at $T_s = 79$ K, and monoclinic crystal symmetry $C2/c$ (17). Kong *et al.* [19] have determined the trigonal structure $R\bar{3}$ (148) at 100 K and suggest a subtle structural phase transition at 78 K. In contrast, Tian *et al.* [20] claim that the structural phase transition of VI_3 is analogous to the structural transition of CrI_3, i.e., between the HT monoclinic structure $C2/m$ (15) (determined at 100 K) and the LT rhombohedral structure $R\bar{3}$ (148) (determined at 60 and 40 K).

The present Rapid Communication is focused on the results of a study of the crystal structures and structural phase transitions in VI_3 by means of x-ray single-crystal diffraction (XRSCD) methods at temperatures between 300 and 5 K, complemented by measurements of specific heat and magnetization as functions of temperature (T) and magnetic field (H).

The refinement of the RT VI_3 crystal structure by the analysis of 792 independent diffraction peaks collected at 250 K provides the trigonal $R\bar{3}$ (148) space group as the best solution. Two possible structure models are suggested in the literature: (a) $R\bar{3}$ (148) [14,19] or (b) $P\bar{3}1c$ (163) [18]. The present refinement of the structure with the space group $R\bar{3}$ (148) quickly converged with excellent R values (see Table S1 in the Supplemental Material [26]) with refined twin-volume fractions. Because some publications report crystal structures of this material based on the Laue symmetry $\bar{3}1m$, refined successfully from powder data, we tried to ignore the R centering and attempted to solve the structure using space group $P\bar{3}1m$ (163). Although the refinement was very unstable and the atomic displacement parameters of iodine atoms mostly wrong, the resulting R value was about 0.06. This demonstrates that even an incorrect structure may provide quite a good fit in the Rietveld refinement. In this case the accuracy is considerably lower compared with the structure determination from single-crystal diffraction data. A detailed description of the RT experiment is presented in the Supplemental Material (SM) [26].

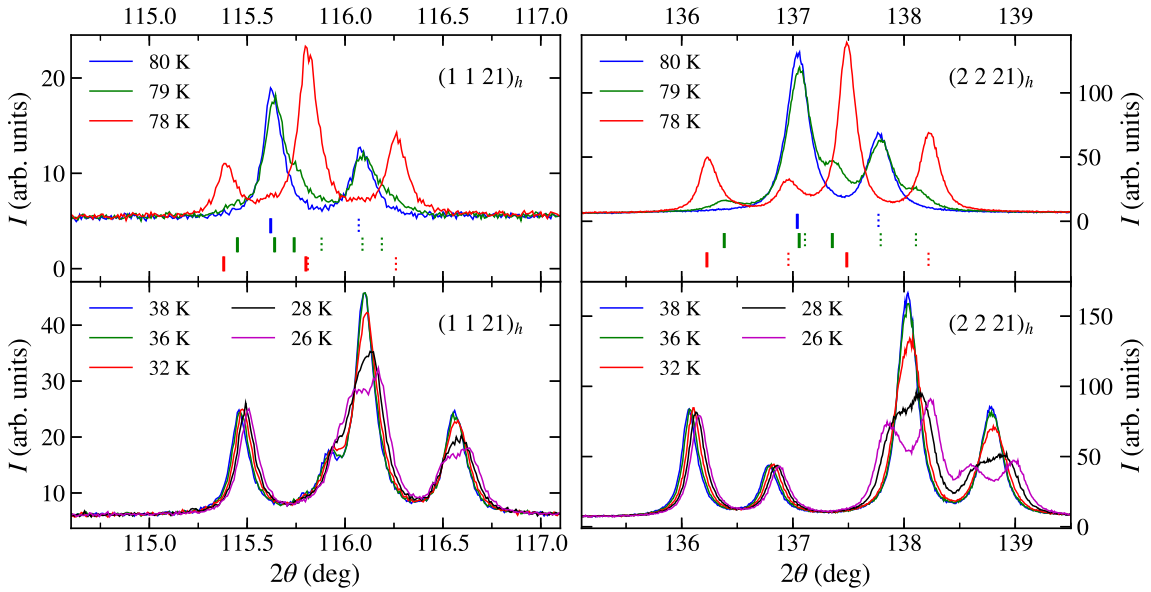

FIG. 1. Evolution of (1 1 21) (left panels) and (2 2 21) (right panels) diffraction peaks of a VI_3 single crystal in the temperature interval from 78 to 80 K (top) and from 26 to 38 K (bottom). The vertical solid and dotted markers indicate the $Cu_{K\alpha 1}$ and $Cu_{K\alpha 2}$ positions of the $Cu_{K\alpha 1,2}$ doublet.

The LT XRSCD measurements evidence that the crystal symmetry is lowered from the HT trigonal symmetry of VI_3 crystals to monoclinic by a structural transition at $T_s = 79$ K. Upon further cooling, another structural transition is observed at 32 K, which causes lowering of the symmetry from monoclinic to triclinic. The transition at 79 K confirms previous reports [18,19] but contradicts the conclusions in Ref. [20]. The structural transition at 32 K is likely related to a transformation of the ferromagnetic structure, which has been recently reported by Gati *et al.* [21] at temperatures below 40 K. In contrast, the monoclinic symmetry remains conserved when VI_3 becomes ferromagnetic below T_{FM1}. Only a change of the temperature dependence of the lattice parameters is observed at temperatures below T_{FM1} which is apparently a result of spontaneous magnetostriction. Our specific-heat measurements revealed that T_s decreases in a magnetic field applied along the trigonal c axis (by almost 3 K in 14 T) whereas it remains intact by the field perpendicular to c. This indicates that a magnetic field applied along the main axis of the VI_6 octahedron, assisted by magnetoelastic interactions, supports the hexagonal symmetry of the V honeycombs in the basal plane of VI_3. It is very likely that strong magnetoelastic interactions should be considered as the main underlying mechanisms driving the structure changes and transitions in VI_3.

The common structural motif of TX_3 compounds is a honeycomb net of T cations as shown in Fig. S1 of the SM [26]. The VI_3 RT trigonal structure of the BiI_3 structure is characterized by the ABC layer stacking sequence. The subsequent layers are shifted along one of the V-V "bonds." The honeycomb net is regular due to the threefold symmetry.

Due to geometrical limitations of the LT diffraction setup and due to the fact that the sample has the shape of a thin (0 0 L) platelet, only diffraction maxima with $L > 0$ can be measured. Therefore, it is not possible to distinguish or determine the exact structure model of VI_3 by mapping selected diffraction peaks, but the temperature dependence of the lattice parameters can be studied.

In this study, we used the hexagonal unit cell for the trigonal crystal system and the corresponding H K L indices. The reciprocal space maps were measured around the symmetric (0 0 24), (0 0 21), (0 0 18), (0 0 15) and asymmetric (2 2 21), (2 2 18), (2 2 15), (1 1 21), (1 1 18), (1 1 15), (4 $\bar{2}$ 21), (4 $\bar{2}$ 18), (4 $\bar{2}$ 15), (2 $\bar{1}$ 21), (2 $\bar{1}$ 15) diffraction peaks. The temperature dependence of the diffraction peaks is shown in Fig. 1. In the trigonal system, the (2 2 L) and (4 $\bar{2}$ L) diffraction peaks have the same 2θ, but a different structure factor, so that the measured intensity ratio $I_{(2221)}/I_{(4\bar{2}21)} \sim 10$ is consistent with the trigonal crystal system. Below 79 K, the (2 2 L) and (4 $\bar{2}$ L) diffraction peaks are both split into two peaks, both split pairs having different 2θ distances (Figs. 1 and 2). An additional diffraction-peak splitting is observed at temperatures below 32 K (Figs. 1 and 2).

The diffraction-peak splitting is ascribed to the reduction of the lattice symmetry. Such a reduction increases the number of nonequivalent diffraction peaks and the diffraction peaks belonging to the more symmetric structure disappear. Therefore, the appearance of the new diffraction peaks by a mere change of extinction rules cannot be explained. From Fig. 2, it is clear that with decreasing temperature one split diffraction peak moves to larger and the other to smaller 2θ values. This fact can be understood by opposite deformation of nonequivalent domains.

The space group of the LT structure is expected to be a maximum *translationengleiche* (t) subgroup of the trigonal crystal system. The trigonal space groups contain only monoclinic and triclinic t subgroups. Two transitions have been observed and, therefore, it is assumed that the monoclinic lattice appears at higher temperatures of 32–79 K and the triclinic one below 32 K. We use the transformation formulas

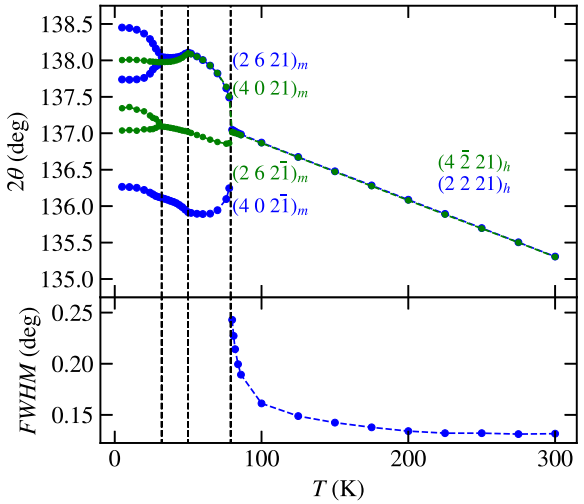

FIG. 2. Temperature dependence of the (2 2 21) and $(4\,\bar{2}\,21)$ diffraction peaks (upper panel) and the diffraction-peak full width at half maximum (FWHM) of (2 2 21) (lower panel). The error bars are smaller than the markers.

in (1) between the hexagonal and monoclinic unit cells, where the indexes h and m stand for hexagonal and monoclinic unit cells, respectively,

$$\boldsymbol{a}_m = \boldsymbol{a}_h, \quad \boldsymbol{b}_m = \boldsymbol{a}_h + 2\mathbf{b}_h, \quad \boldsymbol{c}_m = \boldsymbol{c}_h. \tag{1}$$

The hexagonal and monoclinic basis vectors are sketched in Fig. 3. It is worth noting that if $\beta = 90°$ and $b_m = \sqrt{3}a_m$, the same hexagonal primitive lattice is obtained.

The lattice distortion is connected with the formation of domains in the sample. If we assume only $\beta \neq 90°$ and keep $b_m = \sqrt{3}a_m$, then the diffraction peaks $(2\,2\,L)_h$ and $(4\,\bar{2}\,L)_h$ split into four diffraction peaks: $(2\,2\,L)_h$, $(2\,2\,\bar{L})_h$, $(4\,\bar{2}\,L)_h$, and $(4\,\bar{2}\,\bar{L})_h$, having different 2θ's [$(2\,6\,L)_m$, $(2\,6\,\bar{L})_m$, $(4\,0\,L)_m$, $(4\,0\,\bar{L})_m$ in the monoclinic system]. This assumption is in agreement with observed split pairs $(2\,6\,\bar{L})_m$, $(4\,0\,L)_m$ and $(4\,0\,\bar{L})_m$, $(2\,6\,L)_m$ below 79 K (see Fig. 2). Figure 3 also schematically shows that if β becomes different from 90°, we will see a diffraction peak $(1\,3\,L)_m$ and from another domain the diffraction peak $(2\,0\,\bar{L})_m$ or $(1\,3\,\bar{L})_m$ and $(2\,0\,\bar{L})_m$. On the other hand, the symmetric diffraction peaks (0 0 L) do not

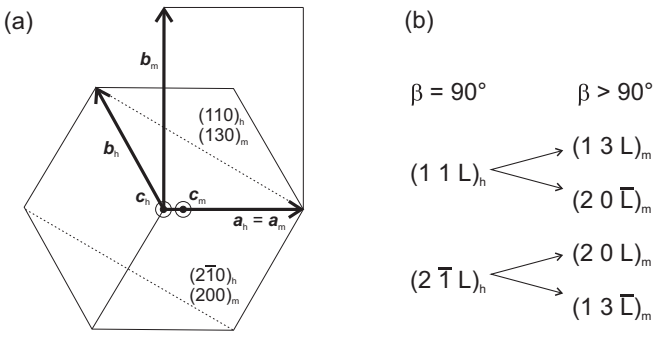

FIG. 3. (a) Schematic representation, basal plane view, of HT and LT unit cells. The indices h and m label the hexagonal and monoclinic unit cell, respectively. (b) Splitting of diffraction if $\beta > 90°$.

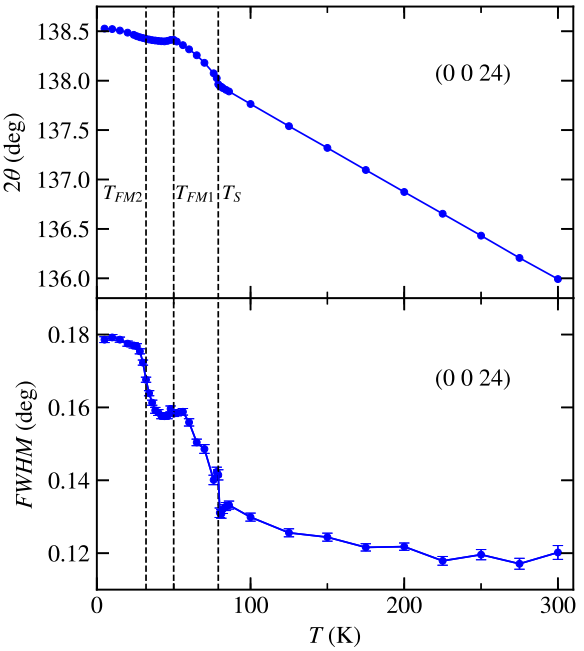

FIG. 4. Temperature dependence of the (0 0 24) diffraction peak (upper panel) and the diffraction-peak full width at half maximum (FWHM) (lower panel).

split, but the transitions are well visible in the change of the slope of the 2θ (T) dependence (Fig. 4).

At RT, the mosaicity of the sample is around 2° (see the high-resolution reciprocal maps in the SM) and therefore is better to integrate the maps in the rocking direction and use only 2θ curves for the determination of the lattice parameters. The correction for the sample displacement $\Delta 2\theta \sim \cos(\theta)$ has been used, which is strictly speaking only valid for symmetric diffraction peaks. Because of the simplicity, we used this correction factor also for asymmetric diffraction peaks. This results in a small systematic error of the lattice parameters, but their temperature dependence remains unaffected. The resulting temperature dependences of the lattice parameters are shown in Fig. 5. A comparison of the measured data and fits is presented in the SM [26].

In Fig. 6, a comparison of the evolution of the specific heat, magnetization, and two diffraction peaks is shown. One can recognize a dramatic splitting of the diffraction peaks coinciding with a sharp specific-heat anomaly at T_s whereas only a negligible change of magnetization was observed at this temperature. The specific-heat and magnetization anomalies at T_{FM1} are well pronounced; no splitting of diffraction peaks is seen, but the character of the temperature dependence of the diffraction angles is changed. Clear additional splitting of certain diffraction peaks, which indicates a lowering of the crystal symmetry from monoclinic to triclinic, is observed below a temperature, which we denote as T_{FM2}(=32 K). Only slight changes in the temperature dependence of the specific heat and magnetization are observed around this temperature.

The decrease of T_s with increasing magnetic field shown in the inset in Fig. 7 seems to be accelerated in fields above 7 T. This is most probably reflecting the enhanced polarization of V paramagnetic moments in high fields. A possibility that it

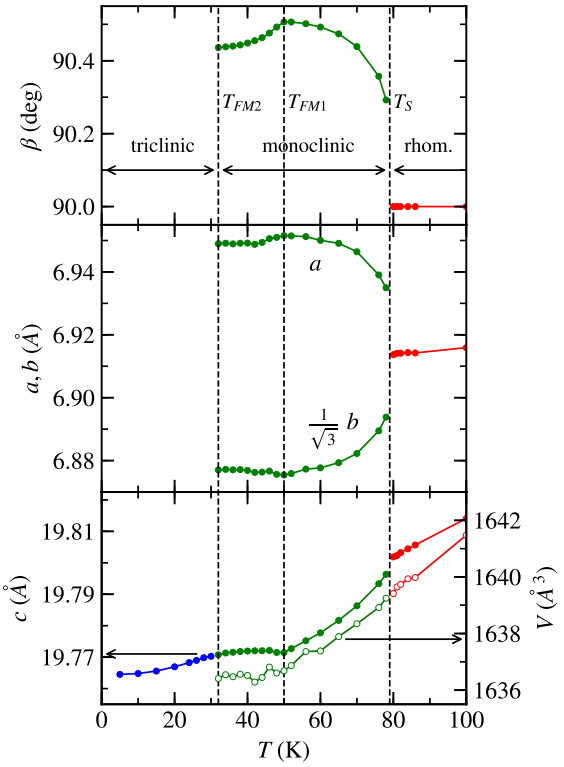

FIG. 5. Temperature dependence of lattice parameters and unit-cell volume of VI_3.

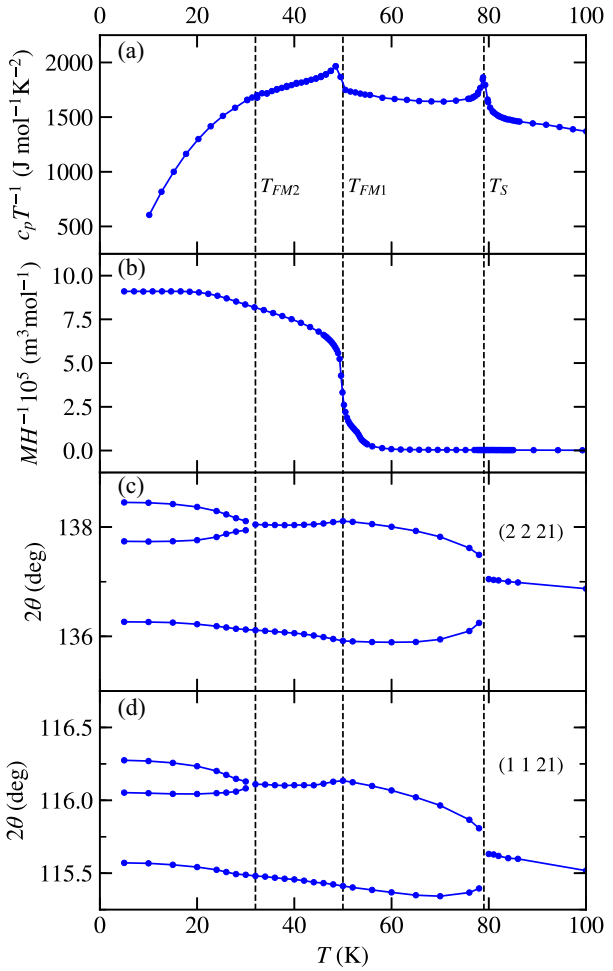

FIG. 6. Temperature dependence of (a) specific heat in a C_p/T vs T plot, (b) c-axis magnetic susceptibility in a magnetic field of 1 mT, and (c) (2 2 21) and (d) (1 1 21) diffraction peaks of a VI_3 crystal.

is due to the C_p anomaly associated with the FM ordering is skewed up in temperature to reach T_s requires more detailed studies of specific heat in magnetic fields.

No field dependence of the anomaly is observed in a field applied within the *ab* plane, as can be seen in Fig. S15 of the Supplemental Material [26].

The RT structure of VI_3, refined from the XRSCD data, is trigonal, which is in agreement with most literature sources [14,15,18,19]. The same $R\bar{3}$ (148) space group has been reported in Refs. [13,15,19]. The trigonal structure persists upon cooling down to 80 K, as evidenced by the unchanged set of measured diffraction peaks. As seen in Fig. 6 and relevant figures in the SM, the temperature dependences of the diffractions angles between RT and 80 K are almost linear.

The sudden splitting of the $(1\,1\,L)_h$ and $(2\,\bar{1}\,L)_h$ diffraction peaks observed upon cooling the VI_3 crystal from 79 to 78 K (see Fig. 6 and relevant figures in the SM [26]) is a result of a structural transition characterized by a lowering of the crystal symmetry, specifically the HT trigonal structure transforms below 80 K to a lower-symmetry structure which can be described by a monoclinic lattice. The transition is the first-order phase transition, because we have observed both the rhombohedral and the monoclinic phases coexisting at 79 K (Fig. 1, top). This coexistence of phases is not compatible with the second-order phase transition. Also, the positions of the diffraction peaks corresponding to the rhombohedral and monoclinic phases are well separated (Fig. 1, top). The transition itself appears as a disappearance of the rhombohedral peak and an appearance of the monoclinic peaks at different 2θ. On the other hand, the temperature cycles around the transition do not show any visible hysteresis (Fig. S16). The lattice parameters a, b, c, and β change abruptly at T_s but the lattice volume remains unchanged.

This structural transition at $T_s = 78$–79 K has been already reported in recent papers [18–21] as accompanied by a sharp specific-heat anomaly and a small negative step in the c-axis magnetization. The measurements of the temperature dependence of the specific heat in the applied magnetic field reveal surprising behavior. T_s is found to be dependent on a magnetic field applied along the c axis, in particular, it is decreased by almost 3 K in 14 T. On the other hand, a field applied in the perpendicular direction has a negligible effect on the T_s-related anomaly. We presume that this behavior is of a magnetoelastic origin and reflects that the magnetic field applied along the axis of the VI_6 octahedra, assisted by magnetoelastic interactions, is protecting the hexagonal symmetry of the honeycomb network in the VI_3 lattice, which leads to the stabilization of the trigonal structure to somewhat lower temperatures.

A transition to the ferromagnetic state is usually accompanied by a subtle distortion of the crystal lattice in zero magnetic field. This spontaneous magnetostriction effect is due to magnetoelastic interactions. This is presumably also

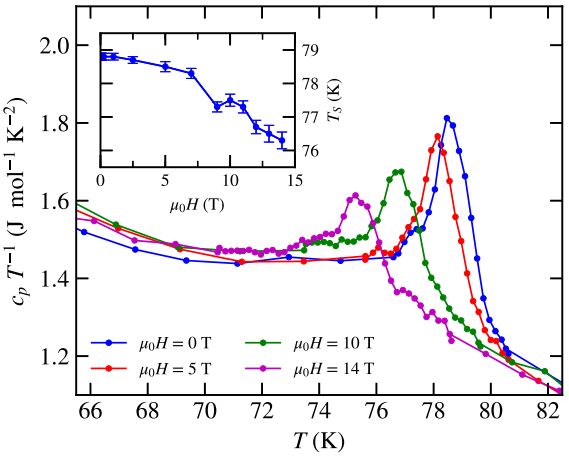

FIG. 7. Temperature dependence of the specific heat (C_p/T vs T plot) of VI_3 in the vicinity of T_s, measured in various magnetic fields applied parallel to the c axis. Inset: Magnetic-field dependence of T_s.

the case in VI_3. In Fig. 5 one can see a slight increase of b and c and decrease a and β, which increases below T_{FM1} towards 90° of the monoclinic structure. The volume magnetostriction between T_{FM1} and 32 K is slightly positive, which is frequently observed in ferromagnets. The distortions induced below T_{FM1} by spontaneous magnetostriction frequently cause symmetry breaking. There are, however, no indications of this in the present study.

However, upon cooling across 32 K, a further lowering of the VI_3 crystal symmetry, namely, from monoclinic to triclinic, is observed. We associate this transition of the VI_3 crystal structure with the transformation of the ferromagnetic structure below 36 K, which has been recently reported by Gati *et al.* [21] from a thorough NMR study. The connections of structural transitions with magnetic phenomena in VI_3 suggest a considerable role of magnetoelastic interactions in this compound. This idea can be further specified when knowing the microscopic aspects of the magnetic structures which are most probably not simple. Somewhat canted ferromagnetic structures have been suggested in previous papers [19,21]. Therefore, investigations focused on the details of the magnetism of VI_3 are strongly desired.

In conclusion, the present extended XRSCD study of the crystal structures and structural phase transitions of the van der Waals ferromagnet VI_3 confirms the existence in three temperature regions and their evolution around phase transitions the existence of the trigonal structure of the $R\bar{3}$ (148) space group at 250 K. Upon cooling, the sudden splitting of certain diffraction peaks at temperatures between 79 and 78 K unambiguously confirms that VI_3 undergoes a structure phase transition between the HT trigonal and the LT monoclinic phase at $T_s \sim 79$ K. The critical temperature of this transition T_s has been found to decrease in magnetic fields applied along the trigonal c axis. Considerable magnetostriction-induced changes of the monoclinic-structure parameters have been recorded below 50 K ($=T_{FM1}$) when VI_3 becomes ferromagnetic. The monoclinic structure transforms upon further cooling into a triclinic variant at 32 K. This transition most probably occurs in conjunction with a transformation of the ferromagnetic structure. These phenomena are associated with a strong magnetoelastic coupling in VI_3. For further understanding of the complex structure and the magnetic phenomena in VI_3, additional experiments at neutron and synchrotron infrastructures focusing on the microscopic aspects of the magnetism are highly desired.

The authors would like to thank Prof. F. de Boer for a critical reading of the manuscript and Dr. V. Petříček for valuable discussions about the peculiarities of trigonal symmetry. This work is a part of the bilateral Czech–Korean research project which is financed by the Czech Science Foundation Grant No. GACR 19-16389J and by Grant No. IBS-R009-G1 provided by the Institute for Basic Science of the Republic of Korea. Most of the experiments were carried out in the Materials Growth and Measurement Laboratory MGML [27] which is supported within the program of Czech Research Infrastructures (Project No. LM2018096). The single-crystal analysis was supported by Project No. 18-10438S of the Czech Science Foundation using instruments of the ASTRA laboratory established within the Operation program Prague Competitiveness, Project No. CZ.2.16/3.1.00/24510.

[1] P. Ajayan, P. Kim, and K. Banerjee, Phys. Today **69**(9), 38 (2016).
[2] K. S. Burch, D. Mandrus, and J.-G. Park, Nature (London) **563**, 47 (2018).
[3] J. Trotter and T. Zobel, Z. Krist.-Cryst. Mater. **123**, 67 (1966).
[4] J.-G. Park, J. Phys.: Condens. Matter **28**, 301001 (2016).
[5] M. McGuire, H. Dixit, V. Cooper, and B. Sales, Chem. Mater. **27**, 612 (2015).
[6] W.-B. Zhang, Q. Qu, P. Zhu, and C.-H. Lam, J. Mater. Chem. C **3**, 12457 (2015).
[7] H. Wang, F. Fan, S. Zhu, and H. Wu, Europhys. Lett. **114**, 47001 (2016).
[8] B. Huang, G. Clark, E. Navarro-Moratalla, D. Klein, R. Cheng, K. Seyler, D. Zhong, E. Schmidgall, M. A. McGuire, D. H. Cobden, W. Yao, D. Xiao, P. Jarillo-Herrero, and X. Xu, Nature (London) **546**, 270 (2017).
[9] J. L. Lado and J. Fernández-Rossier, 2D Mater. **4**, 035002 (2017).
[10] D. R. Klein, D. MacNeill, J. L. Lado, D. Soriano, E. Navarro-Moratalla, K. Watanabe, T. Taniguchi, S. Manni, P. Canfield, J. Fernández-Rossier, and P. Jarillo-Herrero, Science **360**, 1218 (2018).
[11] G. T. Lin, X. Luo, F. C. Chen, J. Yan, J. J. Gao, Y. Sun, W. Tong, P. Tong, W. J. Lu, Z. G. Sheng, W. H. Song, X. B. Zhu, and Y. P. Sun, Appl. Phys. Lett. **112**, 072405 (2018).
[12] A Frisk, L. B. Duffy, S. Zhang, G. van der Laan, and T. Hesjedal, Mater. Lett. **232**, 5 (2018).
[13] Y. Liu and C. Petrovic, Phys. Rev. B **97**, 014420 (2018).

[14] K. Berry, R. Smardzewski, and R. McCarley, Inorg. Chem. **8**, 1994 (1969).
[15] D. Juza, D. Giegling, and H. Schäfer, Z. Anorg. Allg. Chem. **366**, 121 (1969).
[16] J. A. Wilson, C. H. Maule, P. Strange, and J. N. Tothill, J. Phys. C: Solid State Phys. **20**, 4159 (1987).
[17] C. H. Maule, J. N. Tothill, P. Strange, and J. A. Wilson, J. Phys. C: Solid State Phys. **21**2153 (1988) .
[18] S. Son, M. J. Coak, N. Lee, J. Kim, T. Y. Kim, H. Hamidov, H. Cho, C. Liu, D. M. Jarvis, P. A. C. Brown, J. H. Kim, C.-H. Park, D. I. Khomskii, S. S. Saxena, and J.-G. Park, Phys. Rev. B **99**, 041402(R) (2019).
[19] T. Kong, K. Stolze, E. I. Timmons, J. Tao, D. Ni, S. Guo, Z. Yang, R. Prozorov, and R. J. Cava, Adv. Mater. **31**, 1808074 (2019).
[20] S. Tian, J.-F. Zhang, C. Li, T. Ying, S. Li, X. Zhang, K. Liu, and H. Le, J. Am. Chem. Soc. **141**, 5326 (2019).
[21] E. Gati, Y. Inagaki, T. Kong, R. J. Cava, Y. Furukawa, P. C. Canfield, and S. L. Bud'ko, Phys. Rev. B **100**, 094408 (2019).
[22] B. Morosin and A. Narath, J. Chem. Phys. **40**, 1958 (1964).
[23] M. A. McGuire, Crystals **7**, 121 (2017).
[24] W. Klemm and E. Krose, Z. Anorg. Chem. **253**, 218 (1947).
[25] R. E. McCarley, J. W. Roddy, and K. O. Berry, Inorg. Chem. **3**, 50 (1964).
[26] See Supplemental Material at http://link.aps.org/supplemental/10.1103/PhysRevMaterials.3.121401 for details of used methods, room temperature structure, high-resolution XRD, Laue diffraction, LT XRD and specific heat in high magnetic fields.
[27] http://mgml.eu.